Received: 4 March 2020 | Revised: 8 October 2020 | Accepted: 14 November 2020

DOI: 10.1002/we.2599

RESEARCH ARTICLE

WILEY

Active gyroscopic stabilizer to mitigate vibration in a multimegawatt wind turbine

Mehdi Soleymani[1] | Mahdi Norouzi[2]

[1]School of Aerospace, Transport, and Manufacturing. Cranfield University, Cranfield, UK

[2]School of Engineering, Grand Valley State University, Grand Rapids, Michigan, USA

Correspondence
Mahdi Norouzi, School of Engineering, Grand Valley State University, 301 West Fulton Street, Grand Rapids, Michigan 49504, USA.
Email: norouzim@gvsu.edu

Abstract

One of the main concerns in developing large wind turbines, especially offshore, is their cost-effectiveness versus traditional power sources. Significant dynamic loads are applied to the tower and the foundation of a multimegawatt wind turbine. Any reduction in the loads can reduce the size of the structure and, consequently, the turbine's cost. In this paper, a novel structural control application is proposed to mitigate the transmitted vibrations to a multimegawatt turbine tower to decrease the tower base shear forces and overturning moments. For this purpose, a hybrid passive/active gyro stabilizer is designed and incorporated into the NREL baseline 5-MW wind turbine. Furthermore, two controllers, including a proportional integral differential (PID), as the baseline controller, and a nonlinear fuzzy logic controller (FLC) as the main and nonlinear controllers, have been designed and implemented to the turbine model. The structural control systems are implemented into the turbine model by cosimulating ADAMS and Simulink. The results reveal that the application of the proposed stabilizer can significantly reduce the overturning moment at the base of the tower compared to the reference NREL 5-MW model.

KEYWORDS

control, fuzzy control, gysroscopic stabilizier, structure, wind turbine

1 | INTRODUCTION

Global warming and air pollution due to fossil fuels encouraged governments to invest in renewable energy sources in recent years. Wind energy has been the fastest growing renewable energy source globally in the past two decades.[1–3] Many countries across the globe, from Asia to America, have invested in wind energy. The US Department of Energy (DOE) has investigated a roadmap for 35% annual energy supply by wind energy by 2050.[4] Despite short- to medium-term challenges, wind energy will be a viable energy source in the 21st century.

The major drawback of wind energy relative to traditional energy sources is its relatively high cost per kilowatt hour. Wind resources are abundant offshore where the wind is more robust and steadier than land-based wind farms. However, offshore wind farms' deployment, especially in deep waters, is considerably costlier due to the higher cost of foundation, installation, and the required infrastructure to transmit the power to the network. The foundation cost is the most significant single component of the total cost for an offshore wind turbine. Additionally, the foundation has its own installation cost. Any decrease in the foundation size and cost can have a considerable effect on the overall cost of a wind turbine system.[5] According to a US DOE study, the substructure and foundation cost comprises 29.5% of the total cost in a floating offshore wind turbine.[6]

The cost of a foundation for a turbine could be reduced by decreasing the overturning loads applied to the base of the tower. Large-scale wind turbines are tall structures under various ambient and nonambient excitations ranging from the rotor trust force to seismic and wave loads applied to the foundation. In these structures, the stability of the structure and the maximum deflection and overturning moments are primary concerns that must be considered in the design phase.

Structural control systems can efficiently reduce the transmitted vibrations to tall structures such as wind turbines. Structural control systems fall into three categories: passive, semi-active, and active control systems.

In the passive structural control systems, ranging from base-isolation to tuned-mass-damper (TMD) system, tuned liquid column damper (TLDC), and pendulum systems, no external energy is injected into the system. These systems aim at reducing the transmitted energy to the structure by isolating the system from disturbance using a vibration-absorbing mechanism or merely dissipating the transmitted vibrations via a damper (friction and viscous dampers). However, as the vibration absorbing systems' performance depends strongly on their tuning frequency, usually, the structure's fundamental frequency, the mitigation of vibration of higher flexural modes is neglected. The performance of these systems is confined to a very narrow frequency band.

On the other hand, in the semi-active structural control systems, the system's damping or stiffness are controlled parameters. The advantage of semi-active suspension systems is their low energy consumption.

Finally, an active structural control system refers to modifying the structure's response via a controlled force or moment in a closed-loop control system. Among the mentioned systems, the active structural control systems are the most effective ones due to their wide range of operating frequency and efficiency at attenuating the structure's transmitted vibrations. Nevertheless, these systems suffer from high cost and high energy consumption, making them inappropriate for some applications.

The loads applied to a wind turbine structure, and its foundation, could be reduced by using structural control techniques. To this end, the application of a few structural control systems for mitigating wind turbine vibration has been studied by some researchers. However, most of the previous works have been focused on the passive and semi-active structural control systems.

Lackner and Rotea[7] and Stewart and Lackner[8] studied the effect of a one degree-of-freedom (DOF) passive TMD to decrease the vibration on the NREL baseline 5 MW wind turbine. Fitzgerald et al[9] investigated the effect of an active TMD to control the in-plane vibration of wind turbine blades. They used the NREL 5-MW turbine to build a coupled model and reported that the active TMD effectively decreased the blade's vibrations. In another effort, Dinh and Basu[10] investigated the effect of passive single and multiple TMDs to control the vibration of a wind turbine tower and Spar-type floating wind turbines. The TMDs were placed in the spar. They reported that TMD placement in the spar reduced the vibration more effectively compared to a turbine with TMD in the nacelle. Gassempour et al[11] developed an omnidirectional TMD to reduce the vibration in a monopile offshore wind turbine. They showed that due to the structure's nonlinearity, the conventional approach of turning the controller parameters based on the natural frequency of the platform might not be an accurate method to dissipate vibration under normal wind turbine operating conditions. Jahangiri and Sun[12] studied the possibility of using a 3-D pendulum TMD in enhancing the structural integrity of a monopile offshore wind turbine. They also suggested harvesting electricity from the dissipated energy. Jie et al[13] did an experimental study of a ball vibration absorber placed on the top of a scaled wind turbine model in decreasing the vibration of the tower top and the loads applied to the base of the tower. Si et al[14] studied TMD's effect in decreasing a spar floating platform's vibration. They reported that TMD is more effective when placed in the upper part of the spar platform. Zuo et al[15] proposed using multiple TMDs to control a wind turbine tower's vibrations from the fundamental and higher modes of offshore wind turbine towers under the combined wind, sea wave, and earthquake excitations. Their study's main objective was to compare multiple TMDs versus using a single one in controlling the vibrations from various sources of excitation.

Sarkar and Fitzgerald[16] investigated using a passive tuned mass-damper-inerter (TMDI) to control vibration in the tower of a spar-type floating offshore wind turbine. They showed that the TMDI has considerable advantages over the classical TMD. They reported a substantial reduction in the tower vibration in both fore-aft and side-to-side directions under normal and extreme wind and wave conditions. Hu et al[17] proposed an inerter-based structural control system, consisting of a parallel connection of a spring, a damper, and an inerter-based network to mitigate loads in a barge-type floating offshore wind turbine induced by wind and wave. Ma et al[18] introduced a tuned heave plate inerter (THPI) to control heave vibrations in semi-submersible platforms which they showed would outperform a conventional THP This system can potentially be used in offshore wind turbines.

Some efforts have been focused on developing TLCD. Colwell and Basu[19] considered both wind and wave loads on an offshore wind turbine and reported that TLCD could reduce vibration and improve fatigue life significantly. Karimi et al[20] proposed placing a valve-controlled TLCD at the top of a wind turbine tower to decrease its vibration. In more recent work, Buckley et al[21] studied the effect of TLCD both analytically and experimentally using a scaled wind turbine model. They found out that the soil–tower interaction has a considerable impact on the tower's natural frequency and, consequently, the performance of a TLCD.

Other efforts have focused on semi-active algorithms to control the wind turbines. Dinh et al[22] developed a semi-active algorithm using tuned mass damper (TMD) for vibration control of the spar-type floating offshore wind turbine. They reported the semi-active TMD to be more effective than the passive one. Sun[23] used semi-active tuned mass damper (STMD) to mitigate the tower top dynamic response in a monopile offshore wind turbine. He showed that a STMD, retuned in real time, is more effective than a conventional TMD. Sarkar and Chakraborty[24] demonstrated an optimal design of magneto-rheological tuned liquid column dampers (MR-TLCD) for effective wind vibration control of large wind

turbine tower. In other papers, they developed a semi-active strategy using multiple MR-TLCDs to reduce vibration in a multimegawatt wind turbine.[25] They used the NREL 5 MW to demonstrate the performance of their strategy. They concluded that MR-TLCD-based control strategy offers a feasible solution for vibration control of large wind turbines. Hemmati et al[26] proposed a combination of a TLCD with a TMD to minimize vibration in a fixed bottom offshore wind turbine. They considered different loading conditions and concluded that TMDs are more efficient in normal operating conditions, whereas TLCDs perform better in parked conditions.

Few works have been done on the active control of wind turbines' structure. Staino and Basu[27] studied an active rotor speed controller's effect in reducing the blades edgewise vibrations when grid fault occurs Murtagh et al[28] examined the application of the TMD in a wind turbine via simulation and showed that this system could decrease vibrations of the turbine top. Bossanyi[29] studied the benefits of individual blade pitch control versus collective pitch control and reported a significant reduction in the fatigue loads applied to the turbine structure when the blades were controlled individually. Caterino[30] investigated theoretically and experimentally on a scaled model the application of semi-active magnetorheological dampers in decreasing load applied to a base of a wind turbine. Fitzgerald et al[31] proposed incorporating an active TMD into the tower of a wind turbine model. They used the NREL 5-MW turbine to demonstrate their controller's performance and reported a considerable reduction, particularly for high wind speeds, in the tower top fore-aft displacements.

In this study, a methodological approach is proposed to mitigate the transmitted vibrations to the structure of large-scale wind turbines. In this technique, a gyroscopic stabilizer is employed to counteract the transmitted moments to a multimegawatt wind turbine tower. Both passive and active controllers are considered for this purpose. The land-based NREL 5-MW wind turbine is used to demonstrate the efficiency of the proposed system.[32] After describing the turbine and gyroscope models, the controllers' development is explained in the following sections. In the result section, its performance is compared with the original turbine.

2 | MODELING

2.1 | Wind turbine structure

The baseline 5-MW wind turbine developed by the NREL is used in this study.[32] The properties of this model are summarized in Table 1.

The NREL has developed FAST and ADAMS interfacing modules to study the horizontal axis wind turbines for offshore and onshore applications. Figure 1 demonstrates the layout and interconnection between these modules. Table 2 lists the first two natural frequencies of the tower in the fore-aft and side-to-side directions obtained by FAST and ADAMS using the full model of the baseline NREL 5-MW wind turbine model.

TABLE 1 Properties of the NREL baseline 5-MW wind turbine

Rated power, configuration	5 MW, 3-bladed upwind
Control	Variable speed, collective pitch control
Rotor, hub diameter	126 and 3 m
Cut-in, rated, cut-out wind speed	3, 11.4, and 25 m/s
Rated rotor speed	12.1 rpm
Nacelle mass	240 t
Tower mass	347.46 t

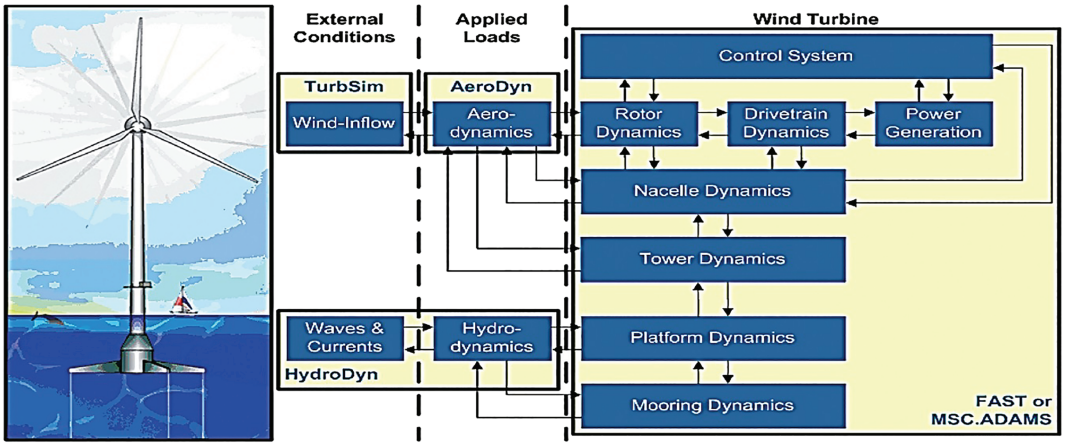

FIGURE 1 Interfacing modules in FAST/ADAMS for analysis of offshore wind turbines[33]

TABLE 2 First two natural frequencies of the tower in fore-aft, side-to-side directions[32]

Description	ADAMS (Hz)	FAST (Hz)
First tower fore-aft mode shape	0.3240	0.3195
First tower side-to-side mode shape	0.3120	0.3164
Second tower fore-aft mode shape	2.9003	2.8590
Second tower side-to-side mode shape	2.9361	2.9408

In this study, two levels of modeling are employed for the turbine structural model. In the first level, which is used for control design purposes, the turbine tower is modeled as a Euler–Bernoulli beam with a concentrated mass on the tip representing the rotor and nacelle. The Euler–Bernoulli's model is validated against the ADAMS model. The Gyrostabilizer is modeled separately, and its equations of motion are coupled to the tower equation. This model, which is called the basic model, will be described below in more detail. A valid full model of the wind turbine developed in ADAMS is utilized to implement the controller at the second level.

The objective of the controller is to mitigate the vibration of the tower under wind loads. To design the controller, using MATLAB, we developed a basic linear beam model by considering three-dimensional Timoshenko beam elements with 12 DOFs. The stiffness and mass matrices ($\mathbf{K}_e$ and $\mathbf{M}_e$), which are used, are included in the appendix.

The NREL baseline 5-MW turbine's tower structure is a tapering hollow cylinder with an outer diameter of 6 and 3.87 m at the base and top of the tower. It is made of steel with a wall thickness of 27 mm at the base and 19 mm at the tower's top.

Similar to the NREL study,[32] the density of 8,500 kg/m^3 and the modulus of elasticity of 210 GPa are considered for the tower. A lumped mass was added, as in Equation 1, to the end of the beam to account for the combined mass of the nacelle and rotor (M = 350 t) (Figure 2).

$$\textit{Tower Mass} = \begin{bmatrix} M & 0 & 0 & 0 & 0 & 0 \\ 0 & M & 0 & 0 & 0 & 0 \\ 0 & 0 & M & 0 & 0 & 0 \\ 0 & 0 & 0 & 0 & 0 & 0 \\ 0 & 0 & 0 & 0 & 0 & 0 \\ 0 & 0 & 0 & 0 & 0 & 0 \end{bmatrix} \tag{1}$$

Table 3 compares the first two natural frequencies of the tower in fore-aft and side-to-side directions with 4 and 20 beam elements. The frequencies converge fast and are relatively close to those obtained for the tower using a full model by FAST or ADAMS. Note that since the beam model is symmetric, the first two natural frequencies in fore-aft and side-to-side directions are identical. However, the first two natural frequencies are slightly different for the full model since the actual 3-bladed turbine is not entirely symmetrical (Table 3).

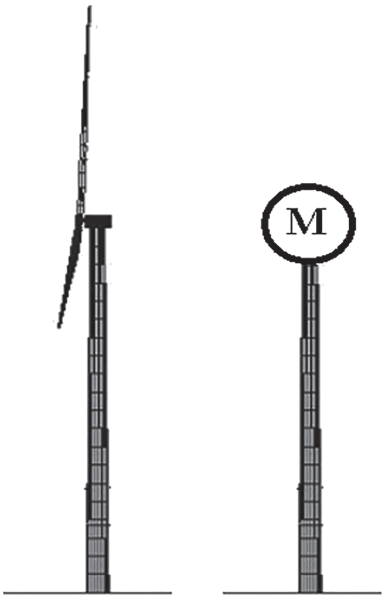

FIGURE 2 Schematic of the model used to tune the controller ($M = M_{\text{Rotor}} + M_{\text{Nacelle}}$)

TABLE 3 First two natural frequencies of the tower using the reduced model by MATLAB

Mode shape	Description	Natural frequency (four elements)	Natural frequency (20 elements)
1	First tower fore-aft	0.2906	0.2957
2	First tower side-to-side	0.2906	0.2957
3	Second tower fore-aft	3.0395	3.0321
4	Secnd tower side-to-side	3.0395	3.0321

The above described linear model is used to design the control parameters. The loads in the fore-aft direction are more significant due to the thrust load applied to the turbine's rotor. The stabilizer's objective is to mitigate the vibration in the fore-aft direction only; therefore, to determine the control parameters, all DOFs in side-to-side directions were suppressed.

After designing the controller, a coupled ADAMS–Simulink model of the NREL wind turbine is developed and used to study the controller's effectiveness. Figure 3 illustrates the layout of the coupled model. FAST was used as a preprocessor to produce ADAMS datasets. Turbsim[34] is used to generate wind speed time series, and AeroDyn is used to calculate the aerodynamic loads applied to the turbine.[35]

2.2 | Gyroscopic stabilizer model

Figure 4 illustrates the basic model and the installed gyroscopic stabilizer schematically. This model, after linearization, is used for the design of the baseline controller. The gyroscopic stabilizer has two DOFs, including the disc's rotation about the axis tangential to the tower at the attachment point and the frame rotation about the axis perpendicular to the disc's rotation axis. In the passive mode, the frame can rotate freely, and therefore, the whole system acts not only as a passive gyro stabilizer but also as a vibration absorber. However, in the active mode, an external torque is applied to the rotating frame, and the frame rotation is controlled while the disc is spinning with a constant velocity.

The governing equations of motion for the passive mode are shown below.[36]

$$\begin{aligned}&\left\{\alpha_1+\alpha_2 v^2+\alpha_3 v^4+\left(G_5+0.5\,{G_5}^3 v^2\right)^2\left[I_o(\cos\theta)^2+I_p(\sin\theta)^2\right]\right\}\ddot{v}+\\&\left\{\alpha_2+2\alpha_3 v^2+{G_5}^3\left(G_5+0.5\,{G_5}^3 v^2\right)\left[I_o(\cos\theta)^2+I_p(\sin\theta)^2\right]\right\}v\dot{v}^2+\\&\left[\alpha_4+\alpha_5 v^2+\alpha_6 v^4\right]v-c^*\dot{v}+\left(G_5+0.5\,{G_5}^3 v^2\right)\left\{(I_p-I_o)\dot{v}\left(G_5+0.5\,{G_5}^3 v^2\right)\dot{\theta}\sin 2\theta+I_p\Omega\dot{\theta}\cos\theta\right\}=0,\end{aligned}\tag{2}$$

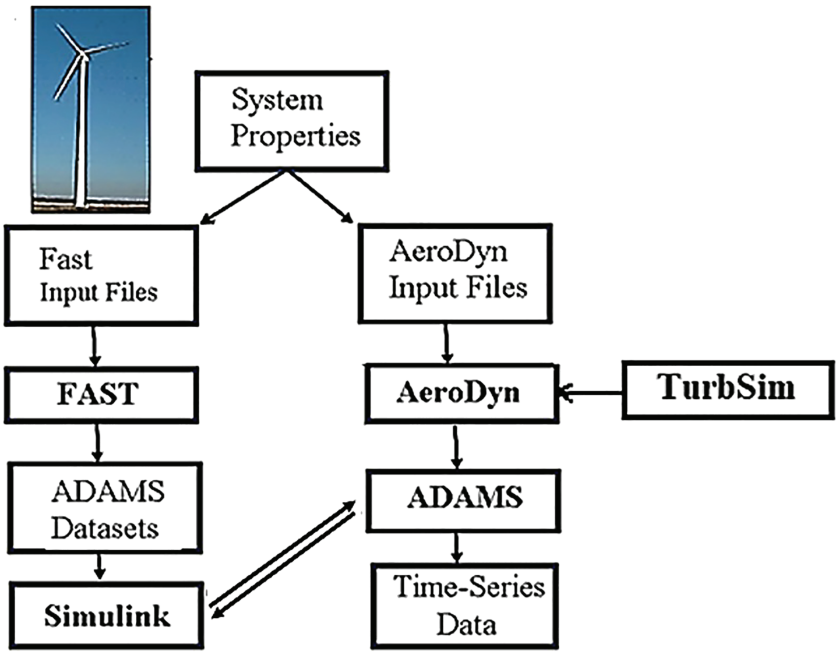

FIGURE 3 Coupled ADAMS–Simulink simulation of a wind turbine

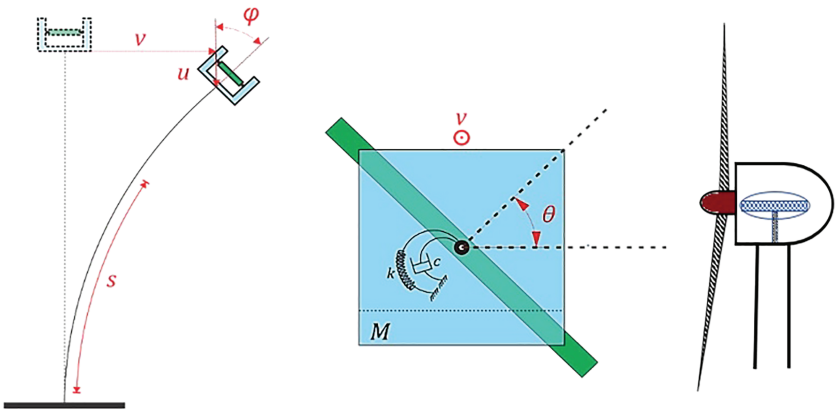

FIGURE 4 Schematic of the model used to tune the controller ($M = M_{Rotor} + M_{Nacelle}$)

$$I_o\ddot{\theta} - \frac{1}{2}(I_p - I_o)\left(G_5\dot{v} + 0.5\,G_5{}^3v^2\dot{v}\right)^2 \sin 2\theta - I_p\Omega\left(G_5\dot{v} + 0.5\,G_5{}^3v^2\dot{v}\right)\cos\theta + c\dot{\theta} + k\theta = T_{Control}, \tag{3}$$

where v and $\dot{v}$ are the displacement and velocity of the tip of the beam, respectively. The angle θ and $\dot{\theta}$ are the rotation angle and angular velocity of the gyro frame, respectively. The tip inclination angle of the beam is indicated by φ, and Ω denotes the angular velocity of the gyro's disk. The α_i and G_i are constant coefficients which depend on the beam geometry and its physical characteristics as follows:

$$G_1 = \int_0^l (\psi(s))^2 ds;\ G_2 = \int_0^l \psi(s) ds;\ G_3 = \int_0^l \left(\int_0^s (\psi'(z))^2 dz\right)^2 ds;\ G_4 = \int_0^l (\psi'(s))^2 ds$$

$$G_5 = \psi'(l);\ G_6 = \int_0^l (\psi''(s))^2 ds;\ G_7 = \int_0^l (\psi'(s)\psi''(s))^2 ds;\ G_8 = \int_0^l (\psi'(s))^4 (\psi''(s))^2 ds;$$

$$G_9 = \int_0^l \left(\int_0^s (\psi'(z))^2 dz\right)^2 ds,$$

where in the above equations $\psi(s)$ is the first mode shape function of the tower with the length, l, defined in terms of position s as below

$$\psi(s) = 1 - \cos\left(\frac{\pi s}{2l}\right).$$

The variables α_1 *to* α_5 are defined as the following:

$$\alpha_1 = \rho A G_1 + m + M + I_t G_5^2;\ \alpha_2 = \rho A G_3 + (m + M) G_4^2 + I_t G_5^4$$

$$\alpha_3 = \frac{1}{4} I_t G_5^6;\ \alpha_4 = EIG_6 - \rho A g G_9 - (m + M) g\, G_4$$

$$\alpha_5 = 2EIG_7;\ \alpha_6 = \frac{3}{4} EIG_8$$

where A is the cross-section area of the tower and ρ, E, I are the density, modulus of elasticity, and the second moment of area of the tower, respectively. The m, M, and I_t are the tower mass, tower top mass, and the moment of inertia of the top mass, respectively.

For the turbine model in this study, the Gs and αs are found in Table 4.

Equations 4 to 6 show the equations of motion in the state-space form.

$$\begin{aligned} \dot{x}_1 &= x_2 \\ \dot{x}_2 &= \Big(-\Big\{\alpha_2 + 2\alpha_3 x_1{}^2 + G_5{}^3\left(G_5 + 0.5\,G_5{}^3 x_1{}^2\right)\left[I_o(\cos x_3)^2 + I_p(\sin x_3)^2\right]\Big\} x_1 x_2{}^2 - \left[\alpha_4 + \alpha_5 x_1{}^2 + \alpha_6 x_1{}^4\right] x_1 - c^* x_2 \\ &\quad - \left(G_5 + 0.5\,G_5{}^3 x_1{}^2\right)\left\{(I_p - I_o) x_2 \left(G_5 + 0.5\,G_5{}^3 x_1{}^2\right)\dot{\theta}\sin 2x_3 + I_p\Omega\dot{\theta}\cos x_3\right\}\Big)/ \end{aligned} \tag{4}$$

TABLE 4 The coefficients in Equations 2 and 3

G_1 (m)	G_2 (m)	G_3 (m^{-1})	G_4 (m^{-1})	G_5 (m^{-1})	G_6 (m^{-1})	G_7 (m^{-5})	G_8 (m^{-9})	G_9 (m^{-1})
19.86	31.83	0.315×10^{-2}	0.141×10^{-1}	0.179×10^{-1}	4.528×10^{-6}	3.640×10^{-10}	5.852×10^{-14}	0.367
α_1 (kg)		α_2 (kg/m^2)		α_3 (kg/m^4)	α_4 (N/m^5)	α_5 (N/m^3)		α_6 (N/m^7)
505,099		97.08		8.908×10^{-6}	1.768×10^{6}	295.98		0.0178

$$\left\{\alpha_1 + \alpha_2 {x_1}^2 + \alpha_3 {x_1}^4 + \left(G_5 + 0.5 {G_5}^3 {x_1}^2\right)^2 \left[I_o(\cos x_3)^2 + I_p(\sin x_3)^2\right]\right\} \tag{5}$$

$$\dot{x}_3 = x_4 \tag{6}$$

$$\dot{x}_4 = \{-0.5\,(I_p - I_o)\left(G_5 x_2 + 0.5\,{G_5}^3 {x_1}^2 x_2\right)^2 \sin 2x_3 - I_p \Omega\left(G_5 x_2 + 0.5\,{G_5}^3 {x_1}^2 x_2\right)\cos x_3 + c x_4 + k x_3 + T_{Control}\}/I_o \tag{7}$$

The system equations are linearized and rewritten in the linear state-space form as follows Equation 8:

The linear model's tip displacement response is compared with that of the nonlinear one for an identical excitation to examine the linear model's accuracy.

Figure 5 compares the linear model's tower-top displacement excited by an Extreme Operating Gust (EOG), with that of the ADAMS nonlinear one. Figure 6 compares the responses under random wind with extreme turbulence. As seen in the figures, the responses agree, implying the linear model's adequacy for tuning the controllers.

The linear model is derived to design the PID controller and is incorporated into the ADAMS/FAST model.

$$\begin{aligned} \dot{X} &= AX + Bu \\ y &= CX + Du \end{aligned} \tag{8}$$

$$A = \begin{bmatrix} 0 & 1 & 0 & 0 \\ -\dfrac{\alpha_4}{{G_5}^2 I_o + \alpha_1} & -\dfrac{c^*}{{G_5}^2 I_o + \alpha_1} & 0 & -\dfrac{G_5 I_p \Omega}{{G_5}^2 I_o + \alpha_1} \\ 0 & 0 & 0 & 1 \\ 0 & \dfrac{G_5 I_p \Omega}{I_o} & -\dfrac{k}{I_o} & \dfrac{c}{I_o} \end{bmatrix}$$

$$B = \begin{bmatrix} 0 \\ 0 \\ 0 \\ -\dfrac{1}{{G_5}^2 I_o + \alpha_1} \end{bmatrix}, \quad C = [1\,0\,0\,0], \quad D = 0.$$

Figure 7 illustrated the gyroscope model in ADAMS, and Table 5 summarizes the mechanical properties of the model, which was incorporated into ADAMS.

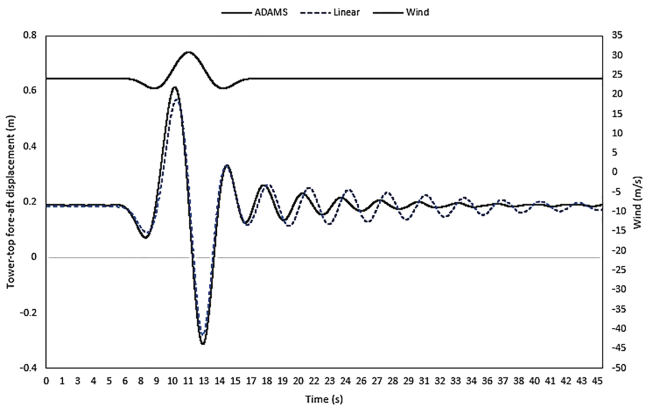

FIGURE 5 Linear versus ADAMS response of the tower under extreme operating gust

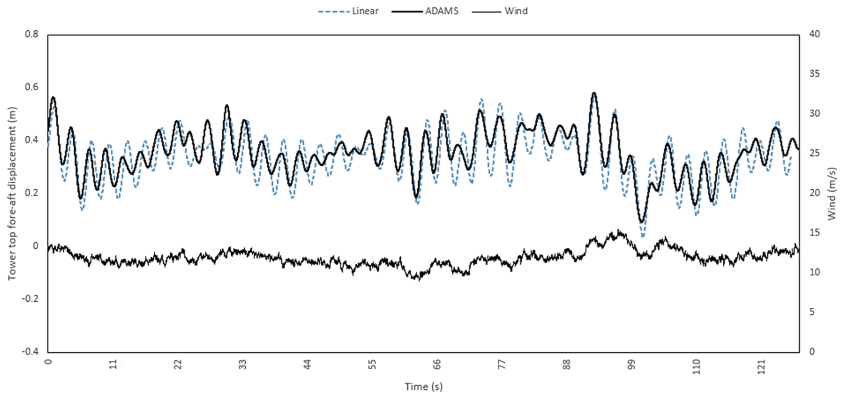

FIGURE 6 Linear versus ADAMS response of the tower under random wind

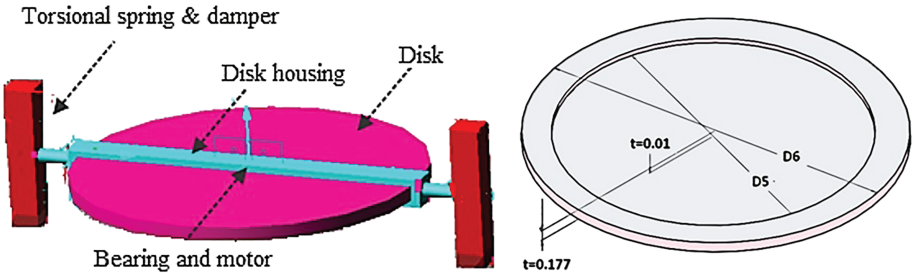

FIGURE 7 The gyroscope disk considered in this design

TABLE 5 Mechanical properties of the gyroscopic model

Mass of the disk	13,459 kg
Outer radius	3 m
Inner radius	2.5 m
Outer ring thickness	17.7 cm
Inner disk thickness	1 cm
Disc mass moment of inertia	95,733 kg/m^2
Material density	7,800 kg/m^3
Spinning velocity	100 (rad/s)
Torsional spring stiffness	100 kN m/rad
Torsional spring damping	297 kN m s/rad

2.3 | Control design and implementation

The objective of the controller is to mitigate the wind-induced turbine's tip displacements. To achieve this goal, two controllers, including a linear PID controller and a nonlinear FLC one, are proposed to be implemented in the turbine model to counteract the wind-induced vibrations via applying a gyroscopic moment to the structure. Figure 8 depicts the schematic diagram for the controllers' implementation.

As it is seen in this figure, the wind load is applied to the primary ADAMS/FAST model as the system disturbance. The ADAMS model is then exported to MATLAB/SIMULINK environment, and the controllers are implemented in the MATLAB model. The response feedback for the controllers is provided by the ADAMS/FAST model via the cosimulation of MATLAB/ADAMS. The control input, in this case, is the frame's input torque ($T_{control}$) applied by a torque actuator. The PID controller's feedback signal is the turbine's tip displacement, and those for the fuzzy controller are tip velocity and displacement. The feedback signals may be calculated by integrating an accelerometer sensor's online data in the turbine's tip. This, of course, may lead to an error in measurement, in case the measured data are contaminated with noise.

The PID controller is designed and tuned based on the linear model but is implemented in the ADAMS model. The signals incorporated in the control design as feedback are turbine's tip displacement and velocity. The practical sensor employed for measuring response variables is a linear accelerometer assumed to be placed in the nacelle. The velocity and displacement feedback are calculated by integrating the acceleration data. This approach for acquitring the required feedback data has some limitations, for example, contamination of the feedback data with the accumulated noise as a result of integration.

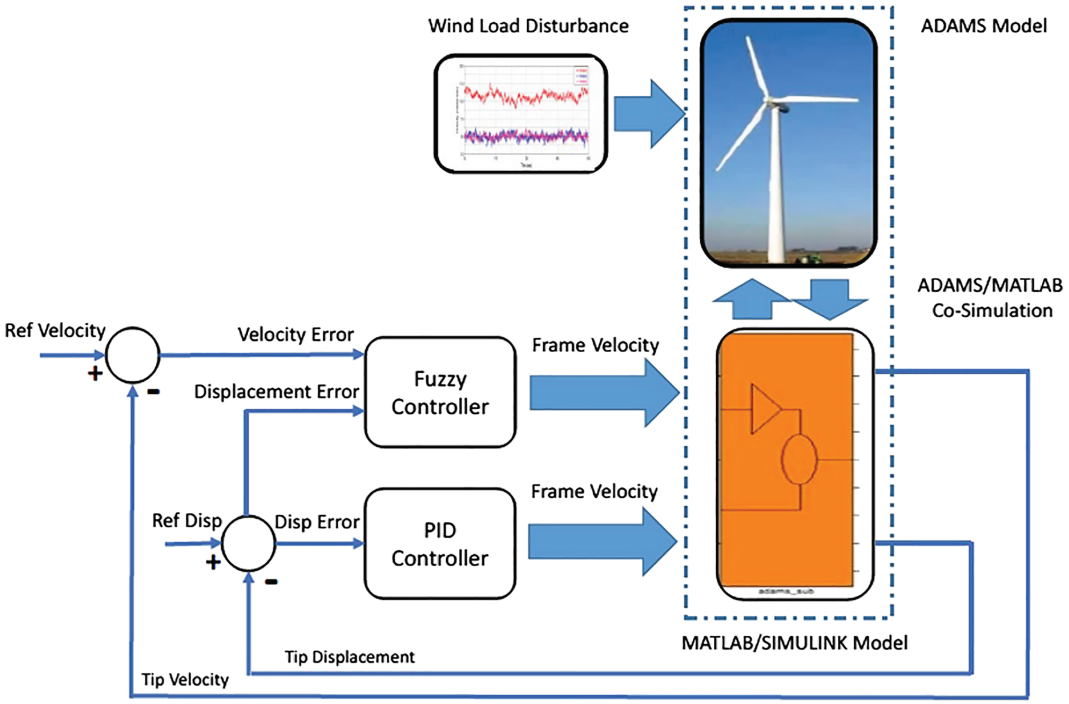

FIGURE 8 Controllers' implementation schematic diagram

The only output parameter employed for the PID controller design is the turbine's tip displacement ($x_1(t)$). For FLC design, as mentioned in Section 2.3.2, two feedback variables, including turbine's tip displacement and velocity ($x_1(t)$, $x_2(t)$). The controllers are described as follows.

2.3.1 | PID controller

The PID controller is designed based on the underlying linear model described in Section 2.1. It is worth mentioning that the designed linear PID controller is not very suitable for controling the original nonlinear model. However, to evaluate the performance of the main controller (FLC), the PID controller is considered a baseline for the comparative study. Thus, the PID controller is designed and tuned based on the linear model but is implemented in the original model (Figure 8). The schematic diagram for the implementation of this controller is shown in Figure 9.

According to this figure, the wind load disturbance is applied to the basic turbine model. The tip displacement feedback is taken away from the reference displacement (zero), and an error signal is generated. The feedback error is then fed to the PID controller, and the gyro's frame input torque is calculated and applied to the model as the control input. Equation 9 depicts the transfer function for the PID controller.

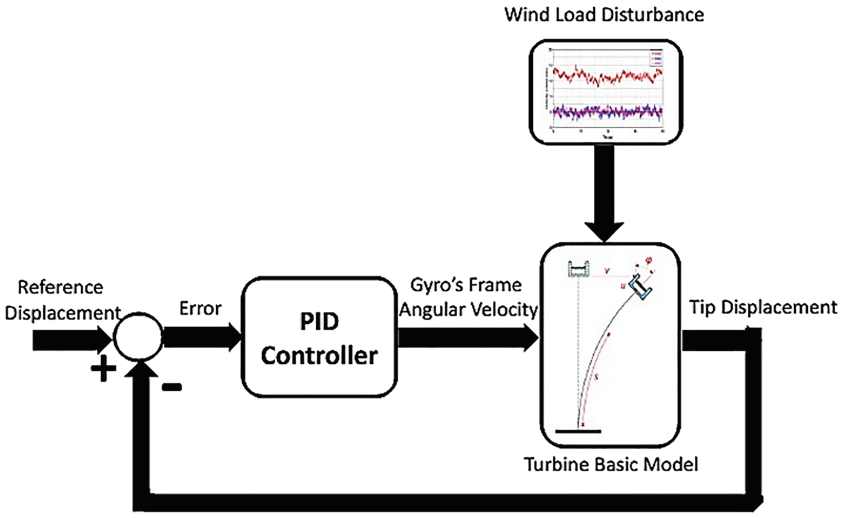

FIGURE 9 Controller schematic diagram

$$u(t) = K_p.e(t) + K_d.\frac{de(t)}{dt} + K_i.\int e(t)dt, \quad (9)$$

where K_p is the proportional coefficient, K_i is the differential coefficient, K_d is the integral coefficient, $e(t)$ is the feedback error (tip displacement), and $u(t)$ is the control input ($T_{control}$).

The PID controller is initially tuned based on Ziegler and Nichols's[37] approach. However, to achieve the desired performance, the controller is further tuned, and its gains are changed so that the desired overshoot and settling time are achieved. For this purpose, a sensitivity analysis is carried out, and various options, including P, PI, PD, and PID controllers, are explored.[38] Table 6 shows the characteristics for some of the controllers considered for this purpose.

Figure 10 also illustrates the tip displacement response to a step input utilizing various controllers.

As seen in this figure, the PID controller's mistuning may result in a high overshoot that is not desirable for the current application. Finally, based on maximum 20% overshoot and reseanable settling time criteria, the tuned PID controller is selected and implemented in the ADAMS model.

2.3.2 | Fuzzy controller

The fuzzy logic controller (FLC) has many advantages,[39] making it a proper match for the current application. First of all, it does not need a mathematical model. This property is beneficial in complicated structural control systems like wind turbines, where the nonlinear ADAMS mathematical models are unavailable, or there are uncertainties in the model parameters. Moreover, there is no limitation for the system nonlinearity. Second, FLC is based on verbose statements, and it is possible to bring the designer's experience into the controller design. Finally, it has inherent robustness, which is vital for uncertain systems.

The proposed FLC is a proportional differential (PD) FLC whose inputs are displacement and velocity of the turbine's tip. The output of the controller is also the frame's input torque. Table 7 depicts the rule bass for the FLC where NB is negative big, NM is negative medium, NS is negative small, and ZE is zero, PS is positive small, PM is positive medium, and PB is positive big.

The rule base has been derived based on engineering judgment and authentic justifications. Let us examine a rule,for example, where the turbine's tip displacement and velocity are both negative big, implying a big deflection and a tendency toward a further displacement. In this case, the controller takes a severe action to counteract the situation, that is, a positive big counteracting torque. Now, let us see another rule where the velocity is negative small. Still, the velocity is positive big, implying a small displacement but a strong desire to return to the equilibrium position.

TABLE 6 Controllers' characteristics and the correposnding linear model responses

Controller	K_p	K_i	K_d	Overshoot (%)	Settling time (s)
P	773,397	0	0	43	4.65
PD	773,397	0	201,075	45	5.15
PI	773,397	580,048	0	31	5.0
PID	773,397	1,160,096	201,075	18	6.1

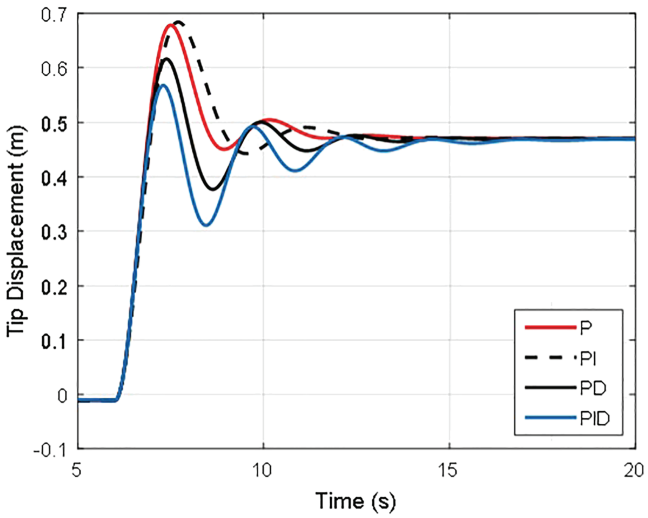

FIGURE 10 Controller schematic diagram

TABLE 7 Rule base of fuzzy logic controller (FLC)

	Turbine tip's displacement				
Turbine tip's velocity	**NB**	**NS**	**ZE**	**PS**	**PB**
NB	PB	PM	PS	ZE	NS
NS	PM	PS	ZE	ZE	NM
ZE	PS	ZE	ZE	ZE	NS
PS	ZE	ZE	ZE	NS	NB
PB	ZE	ZE	NS	NM	NB

Abbreviations: NB, negative big; NM, negative medium; NS, negative small; PB, positive big; PM, positive medium; PS, positive small; ZE, zero.

In this case, the controller decides to take no action, which means a minimum effort to compensate for the condition as the system behavior is desirable. Figure 11A,B shows the membership functions for the inputs and the output, respectively. It is worth mentioning that the membership functions have been distributed uniformly. Therefore, performance of FLC may be further improved by tuning the membership function according to the disturbances.

3 | SIMULATION AND RESULTS

To compare the controller's effectiveness, we study the wind turbine model's behavior under wind loads. The NREL 5-MW model uses a collective pitch control to regulate the power generated by the turbine. The rated wind speed for this model is 11.4 m/s. At this wind speed, the average fore-aft moments become maximum. Above the rated wind speed, the pitch angle is adjusted collectively to reduce the lift loads applied to the rotor, and as a result, the fore-aft bending moment at the base of the tower would decrease.

Based on the IEC61400 standard, the DLC 1.3 load case with an extreme turbulence model is considered to study the gyroscopic stabilizer's performance.[40,41] For the land-based wind turbine, this load case would dominate the design since, due to the high-frequency change in the wind speed, the baseline pitch controller would not be able to react promptly, which would produce large ultimate loads in the turbine structure.[33]

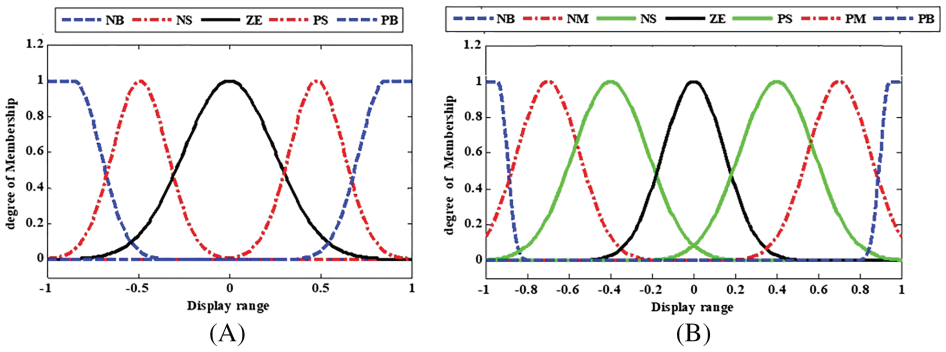

FIGURE 11 (A) Input membership functions and (B) output membership functions

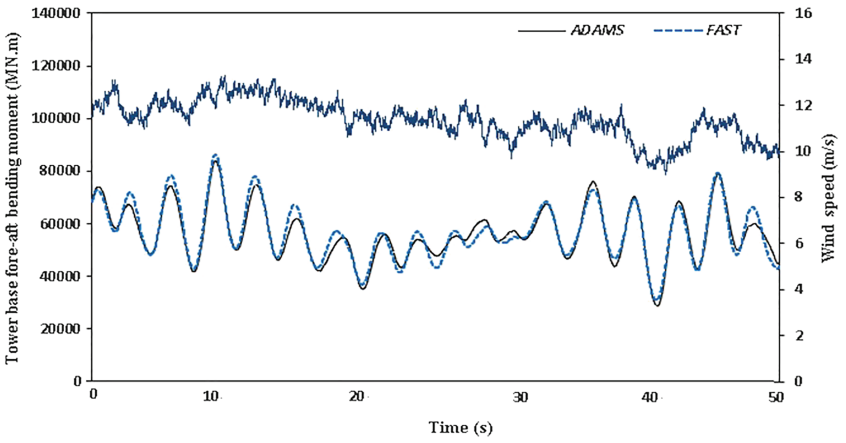

FIGURE 12 Comparison between ADAMS and FAST using original NREL 5-MW turbine

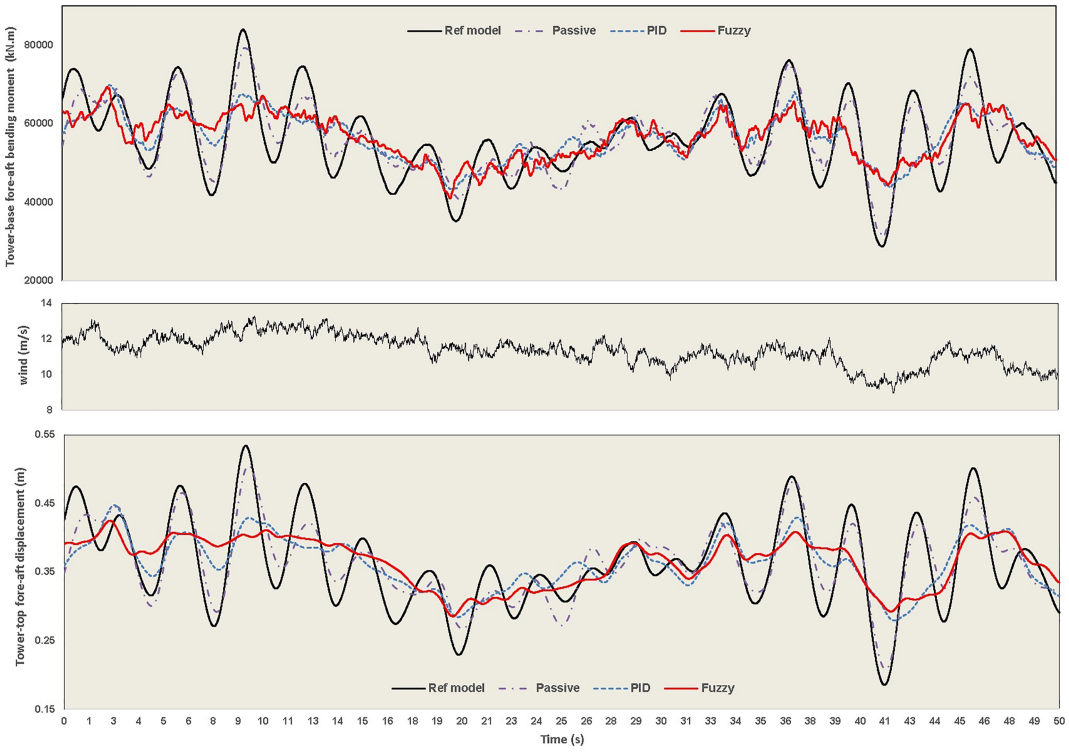

FIGURE 13 Comparison of tower base fore-aft bending moment. Ref. model versus Passive, PID, and fuzzy

Turbsim is used to generate wind time series,[34] and ADAMS/SIMULINK cosimulation is used to obtain the response.[42] To verify the model, we first modeled the turbine using FAST and ADAMS. FAST is an open-source CAE tool developed by the NREL for simulating the coupled dynamic response of wind turbines.[43] Figure 12 compares the response of the reference NREL 5-MW turbine under wind load using ADAMS and FAST. Overall, there is a good agreement between the results of FAST with those of ADAMS.

Figure 13 top compares the tower base overturning moment in the fore-aft direction between the NREL land-based original 5 MW, as a reference, those of model with passive, active PID, and fuzzy gyroscopic stabilizer. The middle figure shows the wind excitation. The lower Figure 13 makes a similar comparison for the tower-top displacement. The active gyroscopes are more effective in decreasing the overturning moments when compared to the passive model. Additionally, the fuzzy controller outperforms the PID one.

Figure 14 shows the root mean square (RMS) and standard deviation (SD) of the fore-aft bending moment, for 10 min, at the base of the tower for the reference model and compares it with those of the turbines equipped with the passive and active PID, fuzzy gyroscopic stabilizers. A considerable reduction in the moment RMS is observed in the turbine with the active gyroscopes. While the passive gyroscope decreases the SD of the moment, the active models' reduction is more substantial than the reference or passive model. Indeed, the fuzzy controller outperforms the PID both in decreasing the RMS and the SD of the bending moment. This can considerably improve the fatigue life of the turbine structure.

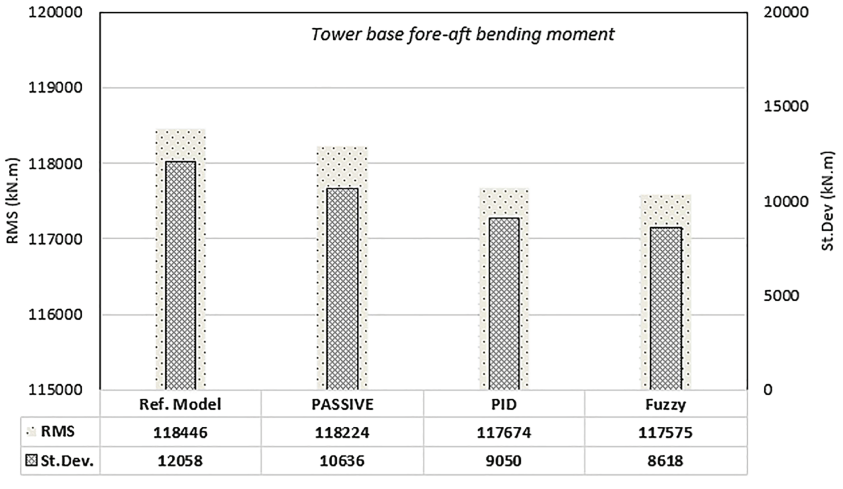

FIGURE 14 Comparison of tower base fore-aft bending moment (RMS and SD)

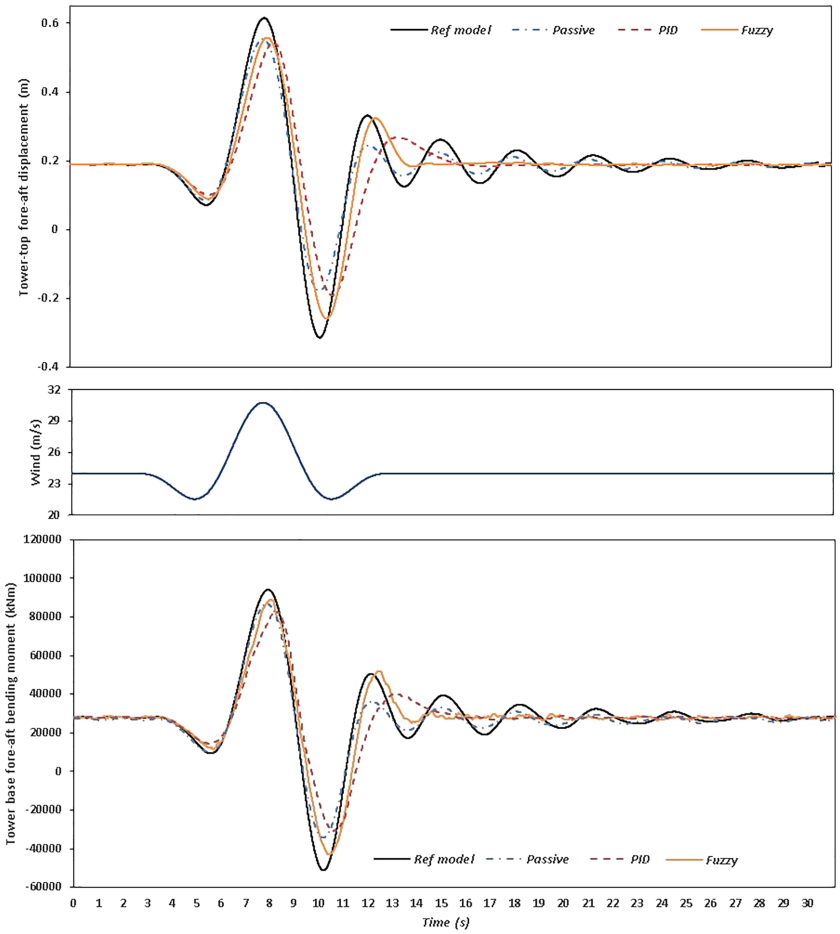

FIGURE 15 Comparison of tower top displacement and its base bending moment in fore-aft direction under extreme operating gust (EOG)

The second load case, which is considered, is the EOG according to IEC standards. In this load case, within 10.5 s, a maximum gust with a speed of 9.16 m/s is added to the wind speed when the turbine is in operating condition at a wind speed 24 m/s. The transient occurs over 10.5 s, and the maximum total wind speed is 33.2 m/s. Figure 15 shows the fore-aft bending moment and the tower top displacement under the EOG load.

As expected, the active gyroscopic stabilizers are more effective than passive ones in decreasing the loads and vibrations. As seen in Figure 15, the fuzzy controller can dissipate the vibration faster than the PID model. However, the drawback of an active gyroscope, when compared to their passive counterpart, is its higher energy consumption.

For the passive gyroscope, initial energy is required for the gyroscope to achieve its design speed (100 rad/s). After that, some energy will be required to overcome the friction to maintain the disk's speed. A higher quality gyroscope would produce less friction, and less power would be spent to maintain its kinetic energy.

For the active gyroscopes, in addition to the power needed to maintain the disk at its rated speed, active energy is required to rotate its frame using a servo-actuator. Figure 16 demonstrates the torque required to control it under the wind load shown in Figure 12. The average power that needs to be spent on the active gyroscopes was estimated to be 250 kW, approximately 5% of the turbine's generated power.

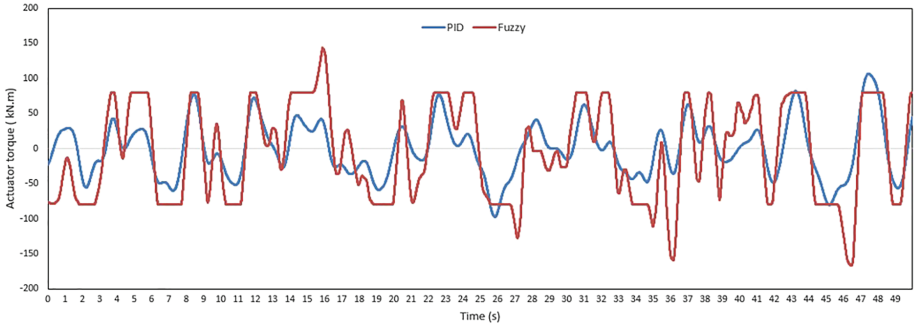

FIGURE 16 Torque required to control the cradle in the active gyroscope

4 | CONCLUDING REMARKS

This study's objective was to investigate the feasibility of passive/active gyroscopic stabilizers in mitigating a multimegawatt turbine's vibration. It was shown that a gyroscopic stabilizer has excellent potential in decreasing the overturning moment applied to the foundation of a turbine. Any reduction in dynamic loads can lead to a lighter design, and a reduction in wind farm's cost would make wind energy more competitive. The active gyroscope stabilizer was more effective in decreasing vibration when compared to the passive one. However, the active system would require more power to operate.

One advantage of a gyroscopic stabilizer, when compared to TMDs, is its relatively lower static weight. In the study by Ghasempour et al,[11] the recommended mass ratio for a TMD system is 5% of the turbine mass, approximately 35 t for the NREL 5-MW turbine. This mass is much greater than the gyro disk's mass, approximately 14 t, considered in this study. Another advantage of a gyrostabilizer is that it can be repositioned relatively easily, to dissipate vibration in other directions (e.g., side-to-side). It is also possible to stack-up gyroscopes to dissipate vibration in different directions. Moreover, unlike TMD and TLCD, this system is not very sensitive to mistuning.

The gyroscopic stabilizer would provide a restraining moment to reduce the vibration of the tower. The moment vector is a free vector, that is, theoretically, the stabilizer's location would not affect its performance. The NREL turbine tower is a tapering tube with 6 m diameter at the base and 4 m diameter at the top. This study's single gyroscope would not fit in the tower; however, one can instead use a series of smaller gyroscopes with equivalent restraining moments that could be fitted inside the tower, perhaps closer to the base of the tower. In this study, similar to other studies cited in this paper,[8,9] the nacelle was considered for the stabilizer position.

The authors believe that a gyroscopic stabilizer is a promising device to mitigate the vibration in large wind turbines. From the standpoint of energy consumption, passive gyro would be a better choice. However, the active gyro is more effective in dissipating the vibration. We believe that a sensible solution would be to utilize the passive gyro to reduce the fatigue loads and engage the active gyro actuators to mitigate severe vibrations whenever needed. The light detection and ranging (LIDAR) technology or other wind forecasting tools make it possible to predict the wind approaching a wind farm, sending a signal to trigger the active control.

More investigation is required to find an optimum gyroscopic stabilizer to find its best layout, minimize its mass, energy consumption, and maximize its effectiveness. According to IEC standards, this must be done by considering different loading conditions, including fault conditions. This, along with the extension of this model to offshore wind turbines, especially floating platforms, is the subject of future research.

ORCID

Mahdi Norouzi https://orcid.org/0000-0002-0262-0399

REFERENCES

1. Policy USEPAOo. *Inventory of US Greenhouse Gas Emissions and Sinks, 1990–1994*. US Environmental Protection Agency, Office of Policy, Planning, and Evaluation; 1995. https://www.epa.gov/ghgemissions/us-greenhouse-gas-inventory-report-archive
2. Administration. UEI. How much of US carbon dioxide emissions are associated with electricity generation? 2017.
3. Energy G. CO2 status report—the latest trends in energy and emissions in 2018. *Int Energy Agency*. 2019.
4. Wiser R, Lantz E, Mai T, et al. Wind vision: a new era for wind power in the United States. *Electr J*. 2015;28(9):120-132.
5. Afjeh AA, Windpower N, Marrone J, Wagner T. *Advanced Offshore Wind Turbine/Foundation Concept for the Great Lakes*. OH (United States): Univ. of Toledo; 2013. https://www.osti.gov/servlets/purl/1227612
6. Moné C, Hand M, Bolinger M, Rand J, Heimiller D, Ho J. *2015 Cost of Wind Energy Review*. Golden, CO (United States): National Renewable Energy Lab.(NREL); 2017. https://www.nrel.gov/docs/fy17osti/66861.pdf
7. Lackner MA, Rotea MA. Passive structural control of offshore wind turbines. *Wind Energy*. 2011;14(3):373-388.
8. Stewart GM, Lackner MA. The impact of passive tuned mass dampers and wind–wave misalignment on offshore wind turbine loads. *Eng Struct*. 2014;73:54-61.
9. Fitzgerald B, Basu B, Nielsen SR. Active tuned mass dampers for control of in-plane vibrations of wind turbine blades. *Struct Control Health Monit*. 2013;20(12):1377-1396.
10. Dinh VN, Basu B. Passive control of floating offshore wind turbine nacelle and spar vibrations by multiple tuned mass dampers. *Struct Control Health Monit*. 2015;22(1):152-176.
11. Ghassempour M, Failla G, Arena F. Vibration mitigation in offshore wind turbines via tuned mass damper. *Eng Struct*. 2019;183:610-636.
12. Jahangiri V, Sun C. Integrated bi-directional vibration control and energy harvesting of monopile offshore wind turbines. *Ocean Eng*. 2019;178:260-269.
13. Jie L, Zili Z, Jianbing C. Experimental study on vibration control of offshore wind turbines using a ball vibration absorber. *Energy Power Eng*. 2012.
14. Si Y, Karimi HR, Gao H. Modelling and optimization of a passive structural control design for a spar-type floating wind turbine. *Eng Struct*. 2014;69:168-182.
15. Zuo H, Bi K, Hao H. Using multiple tuned mass dampers to control offshore wind turbine vibrations under multiple hazards. *Eng Struct*. 2017;141:303-315.
16. Sarkar S, Fitzgerald B. Vibration control of spar-type floating offshore wind turbine towers using a tuned mass-damper-inerter. *Struct Control Health Monit*. 2020;27(1):e2471.
17. Hu Y, Wang J, Chen MZ, Li Z, Sun Y. Load mitigation for a barge-type floating offshore wind turbine via inerter-based passive structural control. *Eng Struct*. 2018;177:198-209.

18. Ma R, Bi K, Hao H. Mitigation of heave response of semi-submersible platform (SSP) using tuned heave plate inerter (THPI). *Eng Struct*. 2018;177:357-373.
19. Colwell S, Basu B. Tuned liquid column dampers in offshore wind turbines for structural control. *Eng Struct*. 2009;31(2):358-368.
20. Karimi HR, Zapateiro M, Luo N. Semiactive vibration control of offshore wind turbine towers with tuned liquid column dampers using H∞ output feedback control, 2010 IEEE International Conference on Control Applications, Yokohama, 2010;2245-2249. https://doi.org/10.1109/CCA.2010.5611186
21. Buckley T, Watson P, Cahill P, Jaksic V, Pakrashi V. Mitigating the structural vibrations of wind turbines using tuned liquid column damper considering soil-structure interaction. *Renew Energy*. 2018;120:322-341.
22. Dinh VN, Basu B, Nagarajaiah S. Semi-active control of vibrations of spar type floating offshore wind turbines. *Smart Struct Syst*. 2016 Oct 1;18(4):683-705.
23. Sun C. Mitigation of offshore wind turbine responses under wind and wave loading: considering soil effects and damage. *Struct Control Health Monit*. 2018 Mar;25(3):e2117.
24. Sarkar S, Chakraborty A. Optimal design of semiactive MR-TLCD for along-wind vibration control of horizontal axis wind turbine tower. *Struct Control Health Monit*. 2018 Feb;25(2):e2083.
25. Sarkar S, Chakraborty A. Development of semi-active vibration control strategy for horizontal axis wind turbine tower using multiple magneto-rheological tuned liquid column dampers. *J Sound Vib*. 2019;457:15-36.
26. Hemmati A, Oterkus E, Khorasanchi M. Vibration suppression of offshore wind turbine foundations using tuned liquid column dampers and tuned mass dampers. *Ocean Eng*. 2019;172:286-295.
27. Staino A, Basu B. Dynamics and control of vibrations in wind turbines with variable rotor speed. *Eng Struct*. 2013;56:58-67.
28. Murtagh P, Ghosh A, Basu B, Broderick B. Passive control of wind turbine vibrations including blade/tower interaction and rotationally sampled turbulence. *Wind Energy*. 2008;11(4):305-317.
29. Bossanyi EA. Individual blade pitch control for load reduction. *Wind Energy*. 2003;6(2):119-128.
30. Caterino N. Semi-active control of a wind turbine via magnetorheological dampers. *J Sound Vib*. 2015;345:1-17.
31. Fitzgerald B, Sarkar S, Staino A. Improved reliability of wind turbine towers with active tuned mass dampers (ATMDs). *J Sound Vib*. 2018;419:103-122.
32. Jonkman J, Butterfield S, Musial W, Scott G. *Definition of a 5-MW Reference Wind Turbine for Offshore System Development*. United States: National Renewable Energy Lab.(NREL), Golden, CO; 2009. https://www.nrel.gov/docs/fy09osti/38060.pdf
33. Jonkman JM. *Dynamics Modeling and Loads Analysis of an Offshore Floating Wind Turbine*. Golden, CO (United States): National Renewable Energy Lab.(NREL); 2007. https://www.nrel.gov/docs/fy08osti/41958.pdf
34. Jonkman BJ. *TurbSim User's Guide: Version 1.50*. Golden, CO (United States): National Renewable Energy Lab.(NREL); 2009. https://www.nrel.gov/docs/fy09osti/46198.pdf
35. Moriarty PJ, Hansen AC. *AeroDyn Theory Manual*. Golden, CO (US): National Renewable Energy Lab; 2005. https://www.nrel.gov/docs/fy05osti/36881.pdf
36. Ünker F, Çuvalcı O. Seismic motion control of a column using a gyroscope. *Procedia Soc Behav Sci*. 2015;195:2316-2325.
37. Ziegler JG, Nichols NB. Optimum settings for automatic controllers. 1993;115(2B):220-222. https://doi.org/10.1115/1.2899060
38. Nagarajaiah S, Reinhorn AM, Constantinou MC. Nonlinear dynamic analysis of 3-D-base-isolated structures. *J Struct Eng*. 1991 Jul;117(7):2035-2054.
39. Chen G, Pham TT, Boustany NM. Introduction to fuzzy sets, fuzzy logic, and fuzzy control systems. *Appl Mech Rev*. 2001 Nov 1;54(6):B102-B103.
40. TC88-MT I. Iec 61400–3: Wind turbines–part 1: Design requirements. *International Electrotechnical Commission, Geneva*. 2005;64.
41. Quarton D. Wind turbines, part 3: design requirements for offshore wind turbines. *Int Electr Com*. 2005.
42. Brezina T, Hadas Z, Vetiska J. Using of Co-simulation ADAMS-SIMULINK for development of mechatronic systems. Paper presented at: 14th International Conference Mechatronika 2011.
43. Jonkman JM, Buhl ML Jr. *FAST User's Guide*. Golden, CO: National Renewable Energy Laboratory; 2005:365-366. https://www.nrel.gov/docs/fy06osti/38230.pdf
44. Craig RR, Kurdila AJ. *Fundamentals of Structural Dynamics*. John Wiley & Sons; 2006. https://www.wiley.com/en-us/Fundamentals+of+Structural+Dynamics,+2nd+Edition-p-9780471430445

How to cite this article: Soleymani M, Norouzi M. Active gyroscopic stabilizer to mitigate vibration in a multimegawatt wind turbine. *Wind Energy*. 2021;24:720–736. https://doi.org/10.1002/we.2599

APPENDIX A.

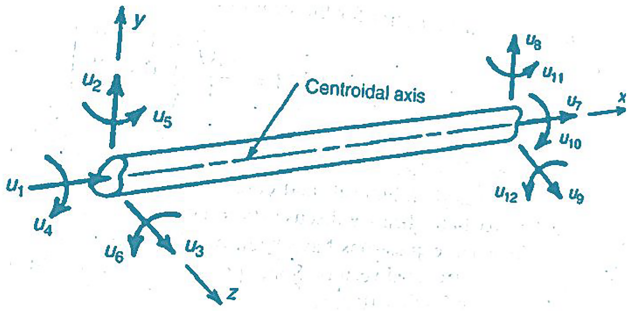

Beam element considered to model the tower.[44]

In the stiffness matrix:

I_y and I_z are the second moments of inertia.

J denotes the polar moment of inertia about x axis.

E and G denote the moduli of Elasticity and rigidity.

A denotes the cross-sectional area of the element.

L is the length of the element

$$[K_e] = \begin{bmatrix} \frac{EA}{L} & & & & S & & & & & & & \\ 0 & \frac{12EI_z}{L^3} & & & & y & & & & & & \\ 0 & 0 & \frac{12EI_y}{L^3} & & & & m & & & & & \\ 0 & 0 & 0 & \frac{GJ}{L} & & & & m & & & & \\ 0 & 0 & -\frac{6EI_y}{L^2} & 0 & \frac{4EI_y}{L} & & & & e & & & \\ 0 & \frac{6EI_z}{L^2} & 0 & 0 & 0 & \frac{4EI_z}{L} & & & & t & & \\ -\frac{EA}{L} & 0 & 0 & 0 & 0 & 0 & \frac{EA}{L} & & & & r & \\ 0 & -\frac{12EI_z}{L^3} & 0 & 0 & 0 & -\frac{6EI_z}{L^2} & 0 & \frac{12EI_z}{L^3} & & & & y \\ 0 & 0 & -\frac{12EI_y}{L^3} & 0 & \frac{6EI_y}{L^2} & 0 & 0 & 0 & \frac{12EI_y}{L^3} & & & \\ 0 & 0 & 0 & -\frac{GJ}{L} & 0 & 0 & 0 & 0 & 0 & \frac{GJ}{L} & & \\ 0 & 0 & -\frac{6EI_y}{L^2} & 0 & \frac{2EI_y}{L} & 0 & 0 & 0 & \frac{6EI_y}{L^2} & 0 & \frac{4EI_y}{L} & \\ 0 & \frac{6EI_z}{L^2} & 0 & 0 & 0 & \frac{2EI_z}{L} & 0 & -\frac{6EI_z}{L^2} & 0 & 0 & 0 & \frac{4EI_z}{L} \end{bmatrix}$$

In the mass matrix:

is the density.

J denotes the polar moment of inertia about x axis.

A denotes the cross-sectional area of the element.

L is the length of the element.

$$[M_e] = \frac{\rho AL}{420}\begin{bmatrix}
140 & & & & S & & & & & & & \\
0 & 156 & & & & y & & & & & & \\
0 & 0 & 156 & & & & m & & & & & \\
0 & 0 & 0 & 140J/A & & & & m & & & & \\
0 & 0 & -22L & 0 & 4L^2 & & & & e & & & \\
0 & 22L & 0 & 0 & 0 & 4L^2 & & & & t & & \\
70 & 0 & 0 & 0 & 0 & 0 & 140 & & & & r & \\
0 & 54 & 0 & 0 & 0 & 13L & 0 & 156 & & & & y \\
0 & 0 & 54 & 0 & -13L & 0 & 0 & 0 & 156 & & & \\
0 & 0 & 0 & 70J/A & 0 & 0 & 0 & 0 & 0 & 140J/A & & \\
0 & 0 & 13L & 0 & -3L^2 & 0 & 0 & 0 & 22L & 0 & 4L^2 & \\
0 & -13L & 0 & 0 & 0 & -3L^2 & 0 & -22L & 0 & 0 & 0 & 4L^2
\end{bmatrix}$$

2020-12-16

Active gyroscopic stabilizer to mitigate vibration in a multimegawatt wind turbine

Soleymani, Mehdi

Wiley

Soleymani M, Norouzi M. (2021) Active gyroscopic stabilizer to mitigate vibration in a þÿ m u l t i m e g a w a t t w i n d t u r b i n e . W i n d E n e r g y , V o l u m e 2 4 , I s s u e 7 , J u l y 2 0 2 1
https://doi.org/10.1002/we.2599